International Journal of Applied Earth Observations and Geoinformation 98 (2021) 102311

Contents lists available at ScienceDirect

International Journal of Applied Earth Observations and Geoinformation

journal homepage: www.elsevier.com/locate/jag

Mapping individual silver fir trees using hyperspectral and LiDAR data in a Central European mixed forest

Yifang Shi [a,*], Tiejun Wang [a], Andrew K. Skidmore [a,f], Stefanie Holzwarth [b], Uta Heiden [b], Marco Heurich [c,d,e]

[a] Faculty of Geo-Information Science and Earth Observation (ITC), University of Twente, Hengelosestraat 99, P.O. Box 217, 7500 AE Enschede, the Netherlands
[b] German Aerospace Center (DLR), Earth Observation Center (EOC), Oberpfaffenhofen, 82234 Wessling, Germany
[c] Department of Nature Protection and Research, Bavarian Forest National Park, Freyunger Str. 2, 94481 Grafenau, Germany
[d] Chair of Wildlife Ecology and Management, University of Freiburg, Germany
[e] Inland Norway University of Applied Science, Institute for Forest and Wildlife Management, Norway
[f] Department of Earth and Environmental Science, Macquarie University, NSW 2109, Australia

ARTICLE INFO

Keywords:
Specific tree species
Silver fir
Hyperspectral
LiDAR
One-class classification

ABSTRACT

Mapping a specific tree species at individual tree level across landscapes using remote sensing is challenging, especially in forests where co-occurring tree species exhibit similar characteristics. In Central European mixed forests, silver fir and Norway spruce have been identified as a pair of coniferous tree species with similar spectral and structural characteristics, typically leading to a major misclassification error in mapping studies. Here, we aimed to accurately map individual silver fir trees in a spruce-dominated natural forest in the Bavarian Forest National Park using integrated airborne hyperspectral and LiDAR data. To accomplish this goal, we extracted a set of relevant spectral and structural features from the hyperspectral and LiDAR data and used them to build machine learning classification models. Specifically, we compared the performance of three one-class classification algorithms (i.e. one-class support vector machine, biased support vector machine, and maximum entropy) for mapping individual silver fir trees. Our results showed that the biased support vector machine classifier yielded the highest mapping accuracy, with the area under the curve for positive and unlabeled samples (*pu*AUC) achieving 0.95 (kappa 0.90). We found that the intensity value of 95th percentile of normalized tree height and the percentage of first returns above 2 m high were the most influential structural features, capturing the main morphological difference between silver fir and Norway spruce at the top tree crown. We also found that the wavebands at 700.1 nm, 714.5 nm, and 1201.6 nm were the most robust spectral bands, which are strongly affected by chlorophyll and foliar water content. Our study suggests that discovering links between spectral and structural features captured by different remotely sensed data and species-specific traits can significantly improve the mapping accuracy of a focal species at the individual tree level.

1. Introduction

Information on tree species composition, distribution, and diversity is of primary significance in the planning and implementation of biodiversity conservation efforts (Suratman, 2012). Accurate tree species mapping is essential for a wide variety of applications, including the mapping of species composition (Cho et al., 2012; Ørka et al., 2013), rare or invasive species detection (Piiroinen et al., 2018; Somers and Asner, 2013a), forest inventories (Bouvier et al., 2015; Yin and Wang, 2016), and biodiversity assessment and monitoring (Baldeck et al., 2015; Vaglio Laurin et al., 2014).

Silver fir (*Abies alba*), native to the mountainous regions of Europe, is considered an important ecological and functional element of European forests for maintaining high biodiversity in forested ecosystems because of its shade tolerance, adaptability to environmental conditions and ability to coexist with many other tree species (Dobrowolska et al., 2017; Tinner et al., 2013). Silver fir is also an important species in the context of climate change, due to its resistance towards natural disturbances and its ability to protect carbon stocks in forests under a warming climate (up to 1300 m^3 of wood per hectare in silver fir forests) (Desplanque

* Corresponding author.
E-mail addresses: y.shi-1@utwente.nl (Y. Shi), t.wang@utwente.nl (T. Wang), a.k.skidmore@utwente.nl (A.K. Skidmore), Stefanie.Holzwarth@dlr.de (S. Holzwarth), uta.heiden@dlr.de (U. Heiden), marco.heurich@npv-bw.bayern.de (M. Heurich).

https://doi.org/10.1016/j.jag.2021.102311
Received 24 June 2020; Received in revised form 11 January 2021; Accepted 31 January 2021

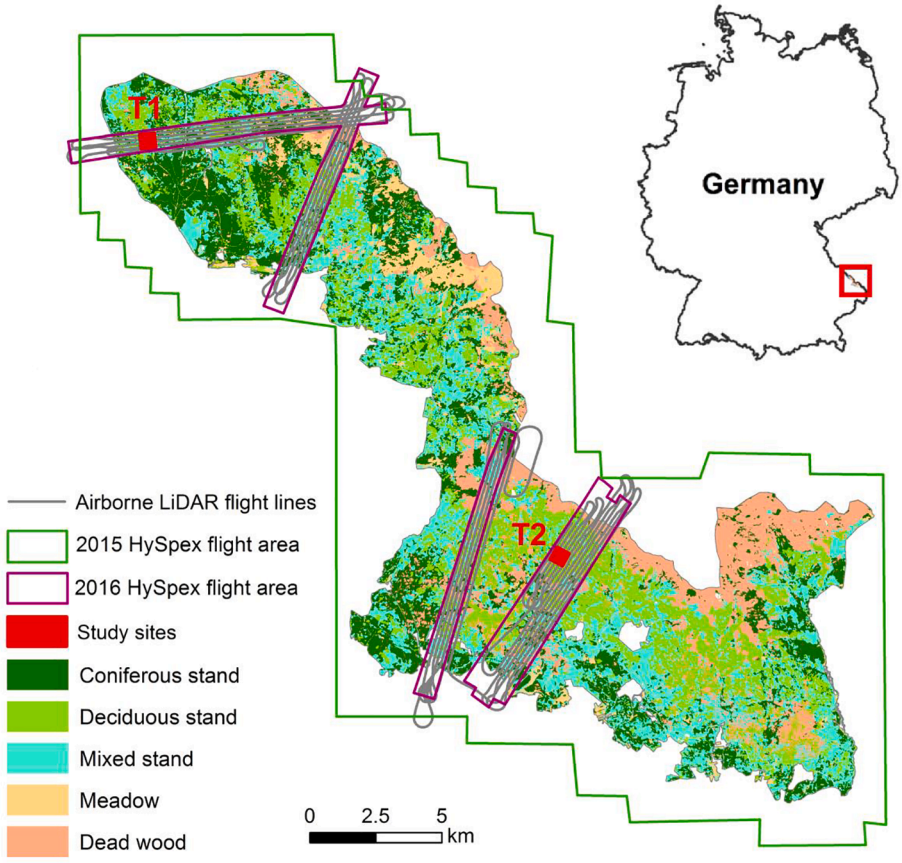

Fig. 1. Airborne LiDAR and HySpex flight area and the location of two study sites in the Bavarian Forest National Park, Germany.

et al., 1999). Furthermore, silver fir forms important protective forests in mountainous areas for infrastructure such as settlements, road, and railways and produces precious timber that is used in construction and furniture (Tinner et al., 2013). However, from the sixteenth century till the twentieth century, a widespread decline of silver fir has been reported in many mountain regions across Europe (e.g. Elling et al., 2009; Ficko et al., 2011; Senn and Suter, 2003; Vrška et al., 2009). For example, in the nineteenth century, the population of silver fir decreased significantly in France and Germany due to the clear cut system. In Franconia (Germany), proportions of silver fir declined from 80% in 1700 to 3% in 1900 (Senn and Suter, 2003). In the Bavarian Forest National Park (BFNP) of Germany, the proportion of silver fir decreased from 60% in 1856 to 3% in 1970 (Heurich and Englmaier, 2010). Silver fir tends to grow as individuals interspersed among other tree species, which makes mapping a particularly challenging task. Furthermore, in Central European mixed forests, silver fir and Norway spruce have been identified as a pair of coniferous tree species with similar spectral and structural characteristics, typically leading to a major misclassification error in related studies (Klopčič et al., 2017; Shi et al., 2018a; Vallet and Pérot, 2011). At this point in time, comprehensive maps of silver fir distribution, or indeed methods to accurately and regularly map this important tree species, are lacking.

The occurrence of individual tree species has conventionally been measured by field sampling, which is accurate but time-consuming and not feasible across large areas. Over the last four decades, advances in remote sensing technologies and machine learning methods have enabled the mapping of individual tree species from different sensor types (Marrs and Ni-Meister, 2019). Both active (Light Detection and Ranging (LiDAR), Synthetic Aperture Radar (SAR)) and passive (multispectral, hyperspectral, thermal) remote sensing systems have been investigated for tree species studies (Ørka et al., 2013; Simard et al., 2000; Skowronek et al., 2018; Vauhkonen et al., 2014). Among those various remotely sensed data, very high resolution aerial photography, UVA-based data, airborne multispectral, hyperspectral and LiDAR data have been widely used for tree species classifications at the individual tree level (reviewed by Fassnacht et al. (2016)). Hyperspectral sensors and Light Detection and Ranging (LiDAR) systems are the most common sources of remotely sensed data used for the classification of tree species (Fassnacht et al., 2016). Hyperspectral sensors measure reflected radiation in hundreds of narrow bands and can detect subtle variations in the biochemical and biophysical properties of the forest canopy (Ferreira et al., 2016; Huber et al., 2008; Somers and Asner, 2013b). LiDAR is an active remote sensing technique that uses lasers to capture the three-dimensional structure of forests. Therefore, it is well-suited for individual tree delineation, while also providing valuable geometric and radiometric information for tree species discrimination (Heinzel and Koch, 2012; Muss et al., 2011; Vauhkonen et al., 2010). To capitalize on the datasets from various airborne sensors and their advantages for individual tree species classification, it is necessary to establish connections between spectral and structural features derived from remote sensing datasets and the species-specific traits of trees. However, an in-depth understanding of how remotely sensed information depicts the species of trees, in other words, how trees display differently in remote sensing data, is still poorly developed.

A framework for multi-class tree species classification requires that representative training data must be collected for every class, regardless of whether a particular class is of interest to the researcher. In the case of remote tree species mapping, collecting adequate amounts of costly field-based training data for all species in an ecosystem is likely to be intractable (Baldeck and Asner, 2015). Consequently, when collected training datasets are not sufficient to adequately characterize every species, understanding of the connection between tree species and remotely senses signatures is limited and the performance of classification is difficult to evaluate. Meanwhile, there is an increasing demand

Table 1
Characteristics of the two study sites.

Study sites	Size (ha)	Elevation (m)	Tree density (per ha)	Soil type	Forest type
T1	25	675–732	445	Brown forest soils and peat soils	Mature coniferous and mixed stands
T2	25	845–906	458	Loose brown soils and gley soils	Mature deciduous and mixed stands

for efficient classification techniques that identify a focal class or species. In this scenario, one-class classification approaches, where labelled data are needed only for the positive class (that is, a single tree species) might be an efficient alternative (Muñoz-Marí et al., 2010). In remote sensing studies, one-class classification approaches have been used to detect focal tree species in tropical rainforests (Baldeck et al., 2015; Somers and Asner, 2013b), invasive species detection (Piiroinen et al., 2018; Skowronek et al., 2017), and high nature value grassland habitats (Stenzel et al., 2017). However, the performance of one-class classifiers is highly dependent on the selection of parameters and thresholds (Waske, 2017). Further comparison of the discriminative potential of different one-class classifiers – that is, the best achievable performance overall models and thresholds – is still needed for accurate tree species mapping.

Instead of focusing on data-driven approaches and pursuing an optimization of classification accuracy of multi-class tree species, as done by many existing studies, we aimed to identify the most relevant species-specific traits for mapping a relatively rare single tree species in a complex temperate forest. The overall objective of this study was to accurately identify and map individual silver fir trees in a spruce-dominated natural forest using airborne LiDAR and hyperspectral data. Specifically, we set out to: (1) generate and select a subset of the most relevant spectral and structural features for silver fir identification, (2) assess the performance of three one-class classifiers for silver fir mapping, and (3) identify the key spectral and structural features that contributed most to the identification of individual silver fir and understand how they link to species-specific traits.

2. Materials and methods

2.1. Study area and tree species

Our experiment was carried out in the Bavarian Forest National Park (49°3′19″ N, 13°12′9″ E), a mixed temperate forest situated in south-eastern Germany (Fig. 1). The park covers an area of 24,218 ha with elevations ranging from approximately 600 m to 1452 m. The mean annual temperature is between 6.5 °C in the valleys and 2 °C at higher elevations, and the climate is continental with an annual precipitation varying from 830 to 2230 mm (Heurich et al., 2010). The dominant tree species in the national park are Norway spruce (*Picea abies*) (67%) and European beech (*Fagus sylvatica*) (24.5%), with sliver fir (*Abies abies*) (2.6%), sycamore maple (*Acer psudoplatanus*) (1.2%), and mountain ash (*Sorbus aucuparia*) (3.1%) contributing to the remainder (Cailleret et al., 2014).

Within the park, two study sites were selected, each approximately 25 ha (500 m × 500 m) (Fig. 1). Detailed information about the two study sites, including elevation, tree density, soil type and forest type is provided in Table 1. The field work was conducted in July 2016 and July 2017, respectively. A Leica Viva GS14 Plus differential GPS (Leica Geosystems AG, Heerbrugg, Switzerland) was used to record the exact location of trees. As a result, 205 locations of trees at site one (T1) and 198 locations of trees at site two (T2) were collected, resulting in 78 beech trees, 58 birch trees, 108 fir trees, 70 maple trees and 89 spruce trees. The collected GPS data was post-processed to obtain differentially corrected coordinates with an accuracy less than 0.5 m.

Table 2
The parameters of HySpex datasets.

Acquisition date	26 August 2015	25 August 2016
Acquisition time (UTC)	10:24	08:51
Flight altitude (m. asl)	3544	2331
Spectral resolution VINR (nm)	3.6	3.6
Spectral resolution SWIR (nm)	6	6
Spatial resolution VNIR (m)	2	1
Spatial resolution SWIR (m)	4	2

2.2. Remote sensing data acquisition and pre-processing

2.2.1. Airborne LiDAR data

The airborne LiDAR data was collected by Milan Flug GmbH on 18 August 2016, covering four transects in the Bavarian Forest National Park (Fig. 1). The Riegl LMS-Q680i scanner (wavelength 1550 nm) integrated in a full-waveform laser scanning system was employed in the campaign, featuring an average point density of 70 pts/m^2, with the mean flight speed at 50 m s^{-1}. The flying altitude was approximately 300 m above ground, with a pulse repetition frequency of 400 kHz.

Both point cloud data generated from Gaussian decomposition (Wagner et al., 2006) and raw full-waveform data were delivered by Milan Flug GmbH (Shi et al., 2018b). Up to eight returns can be recorded for each pulse. The point cloud data composed of planimetric coordinates (x and y), ellipsoidal heights (z), intensity, return number, number of returns, class label, scan angle, echo width, and GPS timestamp of the return (Liu et al., 2018). Both a normalized digital surface model (nDSM) and a canopy height model (CHM) were generated from the LiDAR point cloud data using LAStools software (http://lastools.org/), with a resolution of 0.25 m. The digital surface model (DSM) was normalized by subtracting the elevation of the DSM below each LiDAR point.

2.2.2. Airborne hyperspectral data

Two hyperspectral flight campaigns were carried out by DLR (German Aerospace Centre) with the same HySpex sensor system, developed by Norsk Elektro Optikk (NEO), on 26 August 2015 and 25 August 2016, respectively. The HySpex sensor consists of two imaging spectrometers covering spectral ranges of 400–992 nm (VNIR) and 968–2498 nm (SWIR), with spectral resolutions of 3.6 nm and 6 nm, respectively. The acquisition time, flight altitude, spectral and spatial resolution for each dataset are displayed in Table 2. The HySpex datasets were supplied by DLR after the unified pre-processing procedures (see https://doi.org/10.15489/e8itv4uqol40 for detailed information). The pre-processing procedures included the following steps: radiance conversion and system correction using laboratory radiometric calibration information (Gege et al., 2009); atmospheric correction performed with the ATCOR4 model (Richter and Schläpfer, 2002); *ortho*-rectification of the radiance data based on the parametric model and flight path data in combination with a digital terrain model (DEM) (Müller et al., 2005) and co-registration of VNIR and SWIR data cubes using brisk and sensor-model-based RANSAC (Schwind et al., 2014). A Savitzky-Golay filter was applied to correct for random and systematic noise (Schläpfer and Richter, 2011). After eliminating the bands affected by strong noise or atmospheric effects (water vapour absorption), 290 bands for each dataset remained. Approximately 40 ground control points of each study site were chosen for the co-registration of hyperspectral and LiDAR data using a polynomial warp method (2 degree) and nearest neighbour resampling method in the ENVI software (version 5.2). The resulting geometric accuracy was higher than 0.20 m.

2.2.3. Segmentation of individual trees

The individual tree segmentation was performed using an enhanced

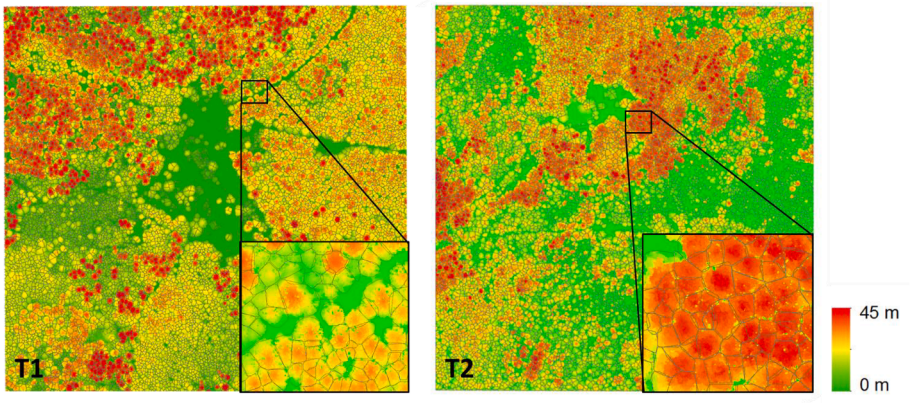

Fig. 2. Segmented individual tree crowns for the two study sites.

Table 3
List of generated LiDAR metrics and hyperspectral features.

Category	Generated features	Definition or formula	Reference
Point distributions	Percent_first	Percentage of first returns above 2 m	(Puttonen et al. 2010)
	Percent_last	Percentage of last returns above 2 m	(Dalponte et al. 2012)
	Percent_all	Percentage of all returns above 2 m	(Korpela et al. 2010)
	Percent_first_mean	Percentage of first returns above mean height	
	Percent_all_mean	Percentage of all returns above mean height	
	All_counts	Total counts of all returns	
	First_counts	Total counts of first returns	
	Counts_returns (1st – 7th)	The counts of different number of returns (1st −7th returns)	
Radiometric metrics	Imean, Isd, Ivar, Icv, Ikur, Iske, Ip_*n*th	Intensity parameters in the tree crown, including mean value (Imean), standard deviation (Isd), variation (Ivar), coefficient variance (Icv), kurtosis (Ikur), skewness (Iske), and *n*th percentile of intensity (5th, 10th, …, 95th, 99th)	(Dalponte et al. 2008) (Yao et al. 2012) (Heinzel and Koch 2011)
	Imean_single, Imean_first	The mean intensity value of single returns (Imean_single), the mean intensity value of the first returns (Imean_first)	
	EWmean, EWsd, EWvar, EWcv, EWkur, EWske, EWp_*n*th	Echo width parameters in the tree crown, including mean value (EWmean), standard deviation (EWsd), variation (EWvar), coefficient variance (EWcv), kurtosis (EWkur), skewness (EWske), and *n*th percentile of echo width (5th, 10th, …, 95th, 99th)	
	EWmean_single, EWmean_first	The mean echo width of single returns (EWmean_single), the mean echo width of the first returns (EWmean_first)	
Geometric metrics	Height, Hmean, Hsd, Hvar, Hcv, Hkur, Hske, Hp_*n*th	Height parameters of the tree, including tree height (Height), mean value (Hmean), standard deviation (Hsd), variation (Hvar), coefficient variance (Hcv), kurtosis (Hkur), skewness (Hske), and *n*th percentile of height (5th, 10th, …, 95th, 99th)	(Li et al. 2013)(Lin and Herold 2016) (Puttonen et al. 2010)
	Hmean_single, Hmean_first	The mean height of single returns (Hmean_single), the mean height of first returns (Hmean_first)	
	CBH:H, C_volume:area, CNR	Ratio of crown base height to height (CBH:H), ratio of crown volume to crown area (C_volume: area), and canopy relief ratio (CNR)	
Band reflectance	B1-B290	Band reflectance from 415.7 to 2496.5 nm	
Vegetation indices	ACI2	Anthocyanin Content Index, ACI2 = ρ650/ρ550	(Gamon and Surfus 1999)
	DWSI2	Disease-Water Stress Index, DWSI2 = ρ1660/ρ550	(Apan et al. 2004)
	RVSI	Red-edge Vegetation Stress Index, RVSI= (ρ714 + ρ752)/2 − ρ733	(Merton 1998)
	SWIR_VI	Shortwave-Infrared Vegetation Index, SWIR_VI = 37.72*(ρ2210-ρ2090) + 26.27*(ρ2280-ρ2090) + 0.57	(Lobell et al. 2001)

3D tree detection algorithm (Yao et al. (2013) (Fig. 2). This object-based algorithm extracts 3D information from the decomposition of full-waveform data and then detects single tree crowns using feature derivation and normalized cut segmentation. A detailed description of the algorithm can be found in Yao et al. (2013).

To match the field samples with the individual 3D LiDAR segmentations, we overlaid the collected GPS tree locations with the crown segments and a georeferenced very high-resolution aerial photograph (0.10 m spatial resolution). We then identified each sample tree by matching it with the crown shape interpreted from the aerial photograph, with the assistance of additional information recorded in the field (e.g. photos of the sample trees and the species of surrounding trees) (Shi et al., 2018b). To reduce linking errors, trees undetected by the segmentation or assigned to more than one segment were removed from further analysis. Finally, we visually verified the identified sample trees that were visible in the two hyperspectral images. In total, 90 fir trees, 77 beech trees, 56 birch trees, 68 maple trees and 88 spruce trees from the two study sites were selected for further analysis. Once the sample trees were verified, the 3D points within each correct segment were extracted and assigned to the corresponding sample trees for the derivation of LiDAR metrics.

2.3. Feature generation

Previous studies demonstrated that sunlit pixels of hyperspectral images can often provide more accurate species information for

classification (e.g. Clark et al., 2005; Dalponte et al., 2013; Richter et al., 2016). To reduce the effect of shadowing, as well as the errors in individual tree crown delineation, we manually selected the sunlit pixels within each tree crown and extracted the spectral information. The mean spectral value of each waveband (B1, B2, …, B290) from each year's hyperspectral data was calculated within each tree crown. Based on the results of our previous study (see Shi et al., 2018a), we also derived four vegetation indices: the Anthocyanin Content Index (ACI2), the Disease-Water Stress Index (DWSI2), the Red-edge Vegetation Stress Index (RVSI), and the Shortwave-Infrared Vegetation Index (SWIR_VI), which is related to plant pigment content, water content and stress (Table 3).

To better understand how LiDAR metrics represent the structural characteristics of tree species, we classified the LiDAR metrics into three primary categories (Table 3). Specifically, these included (1) point distributions, which reflect the structural features of different tree species with the number of laser points tend to decrease from tree top to bottom due to laser obstruction by crowns (Lin and Hyyppä, 2016); (2) radiometric metrics (i.e. intensity and echo width), which suggest that laser amplitudes tend to deteriorate from tree top to bottom, and have different behaviours according to the foliage type, leaf size and density from different tree species; (3) geometric metrics, including tree height, crown shape and crown volume features. The derivation of LiDAR metrics was conducted using the "*rLiDAR*" package in the R language environment (http://www.r-project.org/).

2.4. Feature selection

Feature selection is a procedure that enables a meaningful interpretation of the selected predictors and, in the context of tree species classification, increases the understanding of what exactly drives the discrimination of the species (Fassnacht et al., 2016). To select the most valuable wavebands from the hyperspectral images, we aimed to optimize the spectral separability between fir and other species, and used the principles of the Uncorrelated Stable Zone Unmixing approach proposed by Somers and Asner (2013b) for spectral bands selection. The rationale for this method is to balance the relationship between the spectral separability and the spectral correlation in the final subset (Somers and Asner, 2013b). Firstly, the spectral separability between fir and the other species (i.e. fir and beech, fir and birch, fir and maple, and fir and spruce) was evaluated using the Separability Index (SI), defined as the ratio of the inter-species and the intra-species variability:

$$SI_i = \frac{\Delta_{inter,i}}{\Delta_{intra,i}} = \frac{\left|R_{mean,1,i} - R_{mean,2,i}\right|}{1.96 \times \left(\sigma_{1,i} + \sigma_{2,i}\right)} \quad (1)$$

where $R_{mean,1,i}$ and $R_{mean,2,i}$ are the mean reflectance values at wavelength i for species 1 (i.e. fir) and species 2 (e.g. beech, birch, maple, and spruce), respectively, whereas $\sigma_{1,i}$ and $\sigma_{2,i}$ are the standard deviations of species 1 and 2, respectively. Higher SI values indicate greater separability between the species in the specified waveband (Somers and Asner, 2013b). Secondly, the spectral correlation (*Corr*) of the selected band with all the other wavebands was calculated according to Eq. (2):

$$Corr(X, Y) = \frac{cov(X, Y)}{\sigma_X \sigma_Y} \quad (2)$$

where $cov(X, Y)$ is the covariance between the selected band (X) and the other wavebands (Y), and σ is the standard deviation of the wavebands. Finally, the selection of wavebands was done iteratively by repeatedly selecting the band with the highest separability index and removing the highest correlated band until no bands remained (Somers and Asner, 2014).

To select the final set of features (i.e. from both the hyperspectral and LiDAR metrics) we employed a wrapper algorithm using Support Vector Machines (SVM), a method proposed by Maldonado and Weber (2009). It is based on a sequential backward selection, which uses the number of errors in a validation subset as the measure to decide which feature to remove in each iteration. This approach has several advantages with respect to the objectives of the current study, including (1) it determines the contribution of each feature to the respective classifier, (2) it is capable of measuring the validation error while avoiding overfitting by doing a random split of the dataset in each iteration, and (3) it can be easily generalized to variations of SVM classifiers (Maldonado and Weber, 2009). The feature selection procedure was carried out with the packages "*caret*" and "*e1071*" in the R language environment (http://www.r-project.org/).

Table 4
Description of one-class classifiers.

One-class classifiers	Training mode	Parameters	Tuning settings
OCSVM	*P*-classifier	Sigma (σ): the width of Gaussian radial basis function (RBF) kernel	2^{-10}, 2^{-9}, …, 2^{2}
		Nu (ν): rejection fraction	0.01, 0.02, …, 0.5
BSVM	*PU*-classifier	Sigma (σ): the width of Gaussian radial basis function (RBF) kernel	2^{-4}, 2^{-3}, …, 2^{2}
		cNeg: penalty parameter for unlabeled samples	2^{-7}, 2^{-5}, …, 2^{2}
		cMultiplier: penalty parameter for positive samples	2^{0}, 2^{1}, …, 2^{6}
Maxent	*PU*-classifier	Fc: feature class (lineal (L), quadratic (Q), product (P), threshold (T), and hinge (H))	LQHPT
		Beta (β): regularization multiplier	1, 2, …, 40

2.5. One-class classifiers

Among various one-class classifiers, one-class support vector machine (OCSVM), biased support vector machine (BSVM) and Maxent have been frequently used (Mack and Waske, 2017). The OCSVM (Schölkopf et al., 1999) uses only data from the class of interest to train the classifier, while the BSVM is a semi-supervised classification algorithm that utilizes both positive and unlabelled samples (Liu et al., 2003). The BSVM is a special form of a binary SVM and is adapted to one-class classification with a positive and unlabelled data training set (Stenzel et al., 2017). The Maxent classifier is based on the maximum entropy approach (Sethna, 2006), which is able to perform efficiently even with few occurrence records (Pearson, 2007).

We used only positive and unlabelled data (*PU*-data) during the model training. The spectral features derived from each hyperspectral image, along with the LiDAR metrics, were used in three different one-class modelling approaches, tuned with optimal parameters for fir classification (Table 4). The classification was carried out using the R package "*oneClass*" (Mack, 2015). More information on the kernel parameters, the method and the criteria can be found in the description of the R package "*oneClass*" (*https://github.com/benmack/oneClass*) and the corresponding publication (Mack et al., 2014).

2.6. Accuracy assessment

The classifiers were trained using a 10-fold cross-validation strategy. The training samples were split into ten independent sets (folds), in which nine were used for training and the remaining one for validation. After repeating ten times, the best combination of parameters was chosen by minimizing an average error measurement computed with the predictions on the ten different validation sets (Muñoz-Marí et al.,

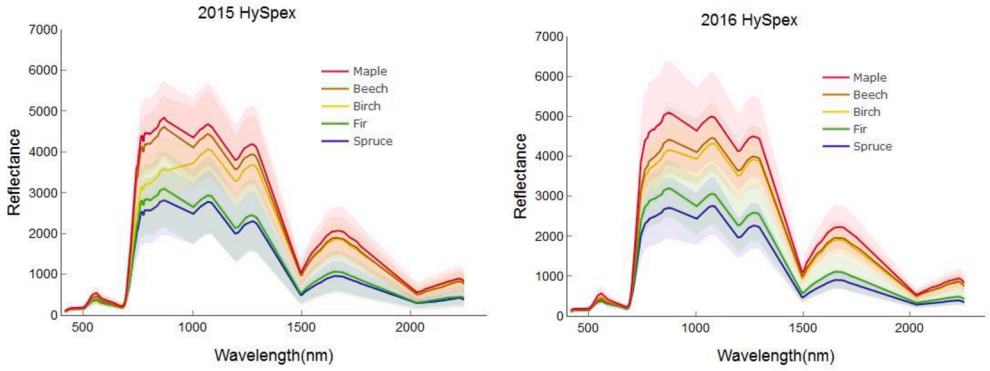

Fig. 3. The mean reflectance value (×1000, ± 1 standard deviation) of five species (beech, birch, fir, maple and spruce) at 400–2498 nm wavelengths derived from HySpex data acquired in 2015 and 2016, respectively.

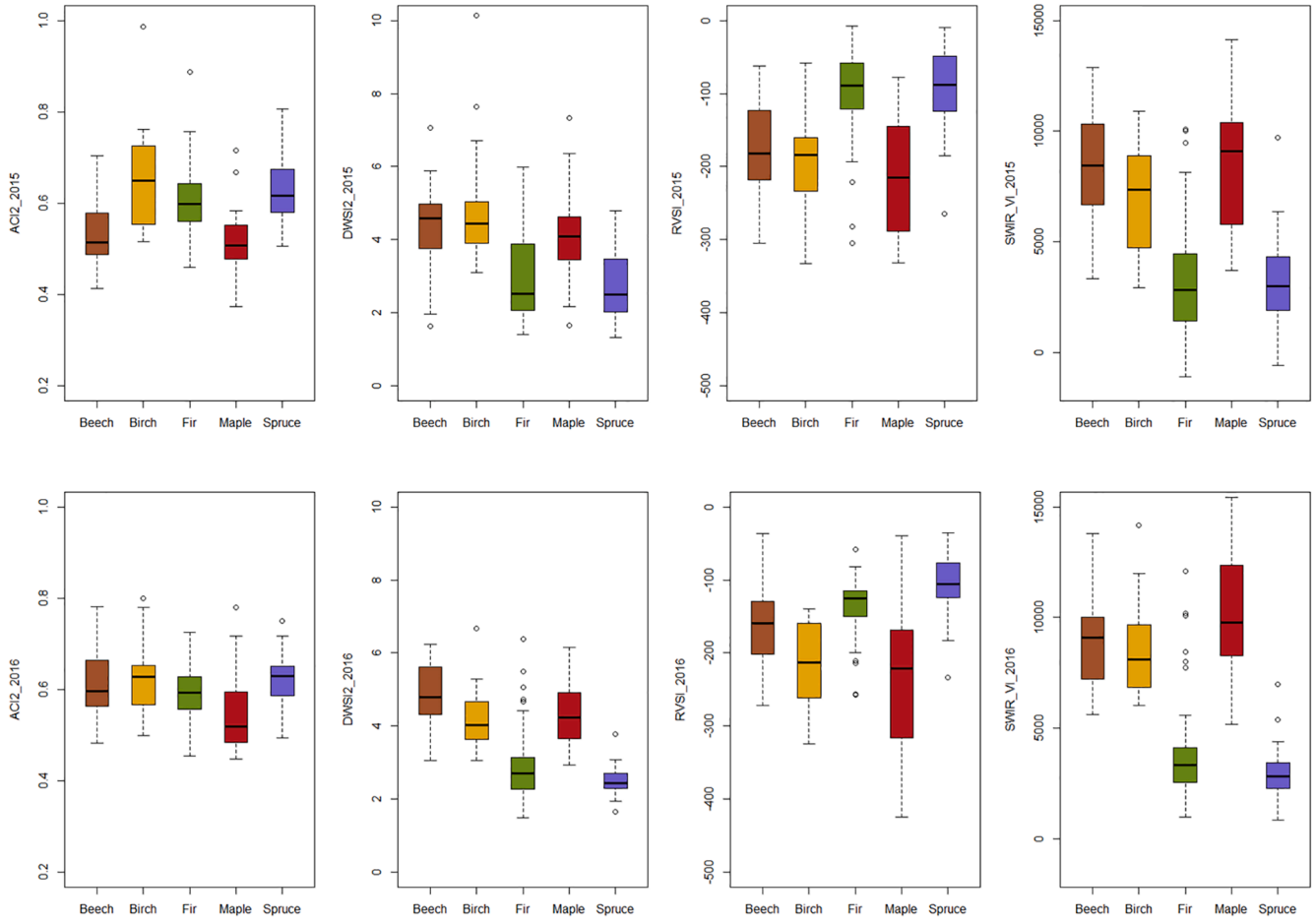

Fig. 4. Box plots of four vegetation indices (i.e. ACI2, DWSI2, RVSI and SWIR_VI) derived from 2015 (first row) and 2016 (second row) among sample tree species.

2010). We selected the best performing model based on the ranking of *pu*AUC (Phillips et al., 2006; Phillips and Dudík, 2008), which resembles the area under the receiver operator characteristic curve (AUC) as an independent measure using randomly sampled observations (Piiroinen et al., 2018). The Kappa coefficient was also measured for each model. In comparative studies, it is rare to see Kappa reported, due to lack of absence samples in the validation data. However, it remains informative since it reveals the relative accuracy of the *PU* data-based model selection approaches (Waske, 2017).

3. Results

3.1. Differences in spectral and structural features between silver fir and four other tree species

Fig. 3 shows the mean spectral signatures (400–2498 nm) of five tree species, derived from the hyperspectral data of 2015 and 2016. The spectral signature of fir is clearly distinguishable from the deciduous trees (i.e. beech, birch, and maple), but the difference between fir and spruce is minor. The difference between the spectral signatures of fir and spruce was larger in the 2016 data than that of 2015.

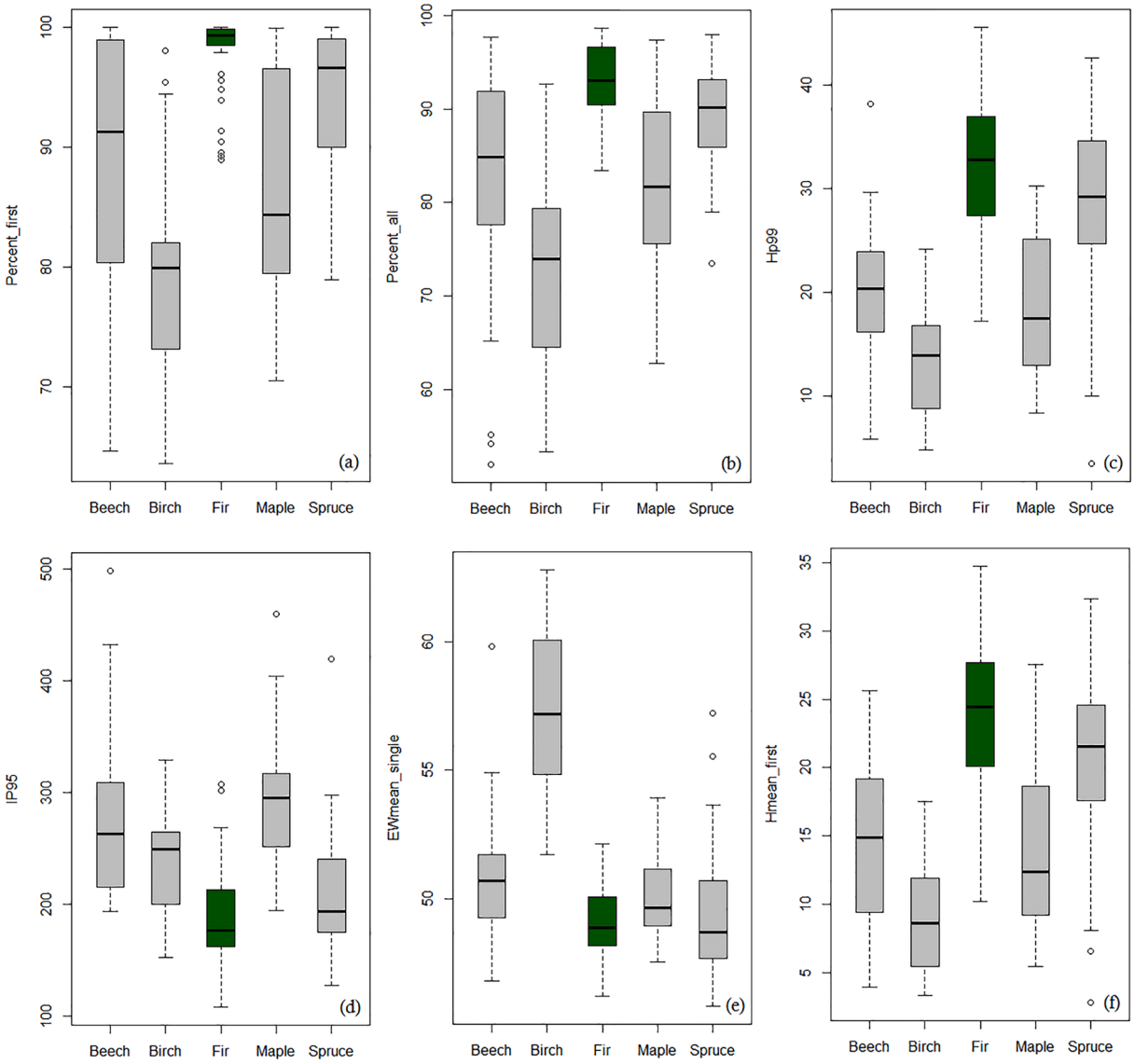

Fig. 5. Box plots of the percentage of first returns above 2 m (a), the percentage of all returns above 2 m (b), 99th percentile of tree height (c), the intensity of 95th percentile of normalized tree height (d), the mean echo width of single returns (e), and the mean height of first returns (f) among sample tree species.

Fig. 4 shows the four vegetation indices (ACI2, DWSI2, RVSI and SWIR_VI), derived from 2015 and 2016, for the five species. The differences between conifers and deciduous trees were more distinct in RVSI and SWIR_VI than in ACI2 and DWSI2. The variation pattern of vegetation indices among the five species was similar in 2015 and 2016, while for each single species, the distribution of vegetation indices varied between 2015 and 2016.

Fig. 5 shows the variation of derived LiDAR metrics between fir and the other four tree species. Six metrics from each LiDAR category (i.e. "Percent_first" and "Percent_all" from point distributions, "Ip95" and "EWmean_single" from radiometric metrics and "Hp99" and "Hmean_first" from geometric metrics) are displayed as examples. Fig. 5a shows that the variation of "Percent_first" (i.e. the percentage of first returns above 2 m) of fir is the smallest among the five species. Fig. 5c and f show distinct differences for the 99th percentile of tree height (Hp99) and the mean height of first returns (Hmean_first) between fir and deciduous trees. However, the differences between fir and spruce were minor.

3.2. Feature selection

Based on the spectral separability and correlation assessment, we selected a set of bands maximizing the separability between each combination of two species. Fig. 6 shows the spectral separability index (SI) between fir and the other four tree species (i.e. maple, beech, birch, and spruce) based on each year of HySpex data. The most distinguishable wavelengths between all pairs were located at 689.3–743.3 nm, 1087.7–1219.6 nm, and 2244.7–2412.6 nm. After feature selection, using the Uncorrelated Stable Zone Unmixing approach and the wrapper SVM algorithm (see Section 2.5), 18 wavebands from the 2015 HySpex, 19 wavebands from the 2016 HySpex, five vegetation indices calculated from both years, and 14 LiDAR metrics, were selected for fir classification (Table 5).

We firstly tested the performance of LiDAR and HySpex data solely for silver fir classification. The selected LiDAR metrics (14), spectral features from 2015 (22), and spectral features from 2016 (23) were used separately as input for three one-class classifiers. The selected spectral features included both band reflectance and vegetation indices. Secondly, we combined the selected LiDAR metrics with spectral features from 2015 and spectral features from 2016 respectively. Given the

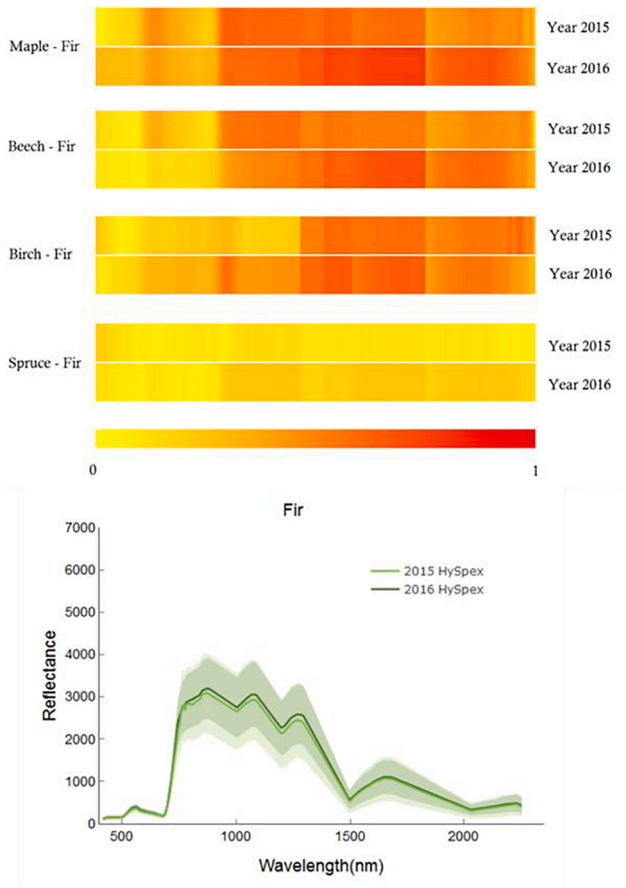

Fig. 6. The upper image shows the spectral separability index (SI) between fir and the other four tree species (i.e. maple, beech, birch, and spruce) in the year of 2015 and 2016. 0 indicates the lowest SI and 1 indicates the highest SI between two species. The lower image shows the mean reflectance value (×1000, ± 1 standard deviation) of fir at 400–2498 nm wavelengths derived from HySpex data acquired in 2015 and 2016, respectively.

similar acquisition dates, we did not combine two HySpex images for the classification of silver fir.

3.3. Performance of classification

Table 6 shows the one-class classification results of silver fir using different dataset and classifiers. Using LiDAR data solely provided slightly higher *pu*AUC and Kappa value than using HySpex data, regardless of the classifier was chosen. Classification using BSVM generated higher accuracy than OCSVM and Maxent when the same dataset was used. The classification result using BSVM with LiDAR and HySpex data from 2016 achieved the highest accuracy (*pu*AUC 0.95 and Kappa 0.90), while the model using LiDAR and 2015 HySpex data had the same *pu*AUC and a slightly lower Kappa value (0.89).

Table 7 shows the significant levels between classification results generated from the combined dataset based on p values in McNemar's test. The classification results from BSVM showed statistically significant improvements compared to the results from OCSVM or Maxent while using the combined LiDAR and HySpex dataset (both from 2015 and 2016).

Fig. 7 shows the normalized importance of selected features (top 20) from hyperspectral and LiDAR data for fir classification. The most important spectral bands for fir classification varied between the different HySpex acquisitions: for 2015, the most important bands were 700.1 nm, 714.5 nm, 1201.6 nm, 1219.6 nm, 2262.7 nm, and 2382.6 nm, while for 2016, the most important bands were 700.1 nm, 714.5 nm, 1201.6 nm, 1591.3 nm, 1723.2 nm, 1771.1 nm, 2070.9 nm. However, there were several bands that were considered important in both years (700.1 nm, 714.5 nm, and 1201.6 nm) (Fig. 7). The percentage of first returns above 2 m (Percent_first) and the intensity of 95th percentile of normalized tree height (Ip95) were the most important LiDAR metrics for fir classification.

Fig. 8 shows the maps of fir trees in two study sites (500 m × 500 m for each site) using BSVM classifier with selected features derived from LiDAR and HySpex data from 2016. The crown of fir trees are highlighted in yellow. The point clouds of mapped fir are highlighted in red.

Table 5
Selected features derived from hyperspectral and LiDAR data.

Input variables	Index or description
LiDAR metrics	
Imean_first	Mean intensity of first-or-single returns
Imean_single	Mean intensity of single returns
Imean	Mean intensity
Ivar	Variation of intensity
Isd	Standard deviation of intensity
Ip95	Intensity of 95th percentile of normalized tree height
EWmean_single	Mean echo width of single returns
EWp55	Echo width of 55th percentile of normalized tree height
Hmean_first	Mean height of first-or-single returns
Hmean_single	Mean height of single returns
Hvar	Variation of height
Hp99	99th percentile of normalized tree height
Percent_first	Percentage of first returns above 2 m
Percent_all	Percentage of all returns above 2 m
Spectral features (HSI)	
Band reflectance (nm)	
2015 HySpex	415.7 nm, 433.7 nm, 502.1 nm, 527.3 nm, 692.9 nm, 700.1 nm, 714.5 nm, 732.5 nm, 764.9 nm, 872.9 nm, 1201.6 nm, 1219.6 nm, 1597.3 nm, 2106.8 nm, 2262.7 nm, 2382.6 nm, 2400.6 nm, 2418.6 nm
2016 HySpex	419.3 nm, 437.3 nm, 458.9 nm, 678.5 nm, 689.3 nm, 692.9 nm, 700.1 nm, 707.3 nm, 714.5 nm, 746.9 nm, 854.9 nm, 883.7 nm, 1195.6 nm, 1591.3 nm, 1723.2 nm, 1771.1 nm, 2070.9 nm, 2406.6 nm, 2412.6 nm
Vegetation Indices	
ACI2	ACI2 = ρ650/ρ550
SWIR_VI	SWIR_VI = 37.72*(ρ2210-ρ2090) + 26.27*(ρ2280-ρ2090) + 0.57
DWSI2	DWSI2 = ρ1660/ρ550
RVSI	RVSI= (ρ714 + ρ752)/2 − ρ733

4. Discussion

This study accurately mapped individual silver fir trees in a Norway spruce dominated forest using one-class classification methods, employing key spectral and structure features closely linked to species-specific traits. Results of this study demonstrate that the biased support vector machine classifier yielded the highest mapping accuracy, with the area under the curve for positive and unlabeled samples (*pu*AUC) achieving 0.95 (kappa 0.90).

Identifying key features that can reflect the specific traits of tree species is an important issue for tree species classification. Our study revealed that the most robust spectral bands from HySpex datasets for mapping of silver fir were located at wavebands 700.1 nm and 714.5 nm, which are strongly affected by leaf chlorophylls (Ustin et al., 2009), as well as the waveband of 1201.6 nm, which is sensitive to foliar water content (Kokaly et al., 2009). This result is in line with Gitelson et al. (2003) and Ustin et al. (2009), who indicated that the total chlorophyll content in leaves is closely related to the green (540–560 nm) and red edge (700–730 nm) wavelengths. In the study of Shi et al. (2018a), conducted in the same study area, leaf chlorophyll (Cab) and equivalent water thickness (Cw) were measured from field samples of five tree species (i.e. beech, birch, fir, maple and spruce); fir showed the highest leaf chlorophyll (mean: 56.3 μg cm^{-2}, sd: 11.0 μg cm^{-2}) and equivalent

Table 6
One-class classification results of fir trees from hyperspectral and LiDAR data using three different classifiers.

	LiDAR		2015 HySpex		2016 HySpex		LiDAR + 2015 HySpex		LiDAR + 2016 HySpex	
	*pu*AUC	Kappa	*pu*AUC	Kappa	*pu*AUC	Kappa	*pu*AUC	Kappa	*pu*AUC	Kappa
OCSVM	0.72	0.61	0.68	0.58	0.70	0.60	0.89	0.87	0.90	0.87
BSVM	0.75	0.62	0.70	0.60	0.73	0.61	0.95	0.89	0.95	0.90
Maxent	0.67	0.56	0.59	0.48	0.66	0.55	0.83	0.82	0.87	0.85

Table 7
McNemar's test for pairwise comparison between classification results using different classifiers. NS: $p > 0.05$. ***$p < 0.001$.**$p < 0.01$. *$p < 0.05$.

	LiDAR + 2015 HySpex		LiDAR + 2016 HySpex	
	OCSVM	Maxent	OCSVM	Maxent
BSVM	*	**	*	*
Maxent	*	–	NS	–

water thickness (mean: 0.0166 cm; sd: 0.0012 cm) among the five tree species. Norway spruce, as the other conifer, caused the main confusion in fir classification. However, it showed a comparatively low leaf chlorophyll (mean: 34.5 μg cm^{-2}, sd: 6.4 μg cm^{-2}) and equivalent water thickness (mean: 0.0140 cm; sd: 0.0024 cm). This highlights that optimizing spectral separability between the focal tree species and others can help discriminating them, since absorption features caused by biochemical composition control the shapes of leaf reflectance spectra. It is worth noting that the specific wavebands that contribute most in a focal species mapping are highly depend on the species of interest and the neighboring species (e.g. the species with similar reflectance) as well

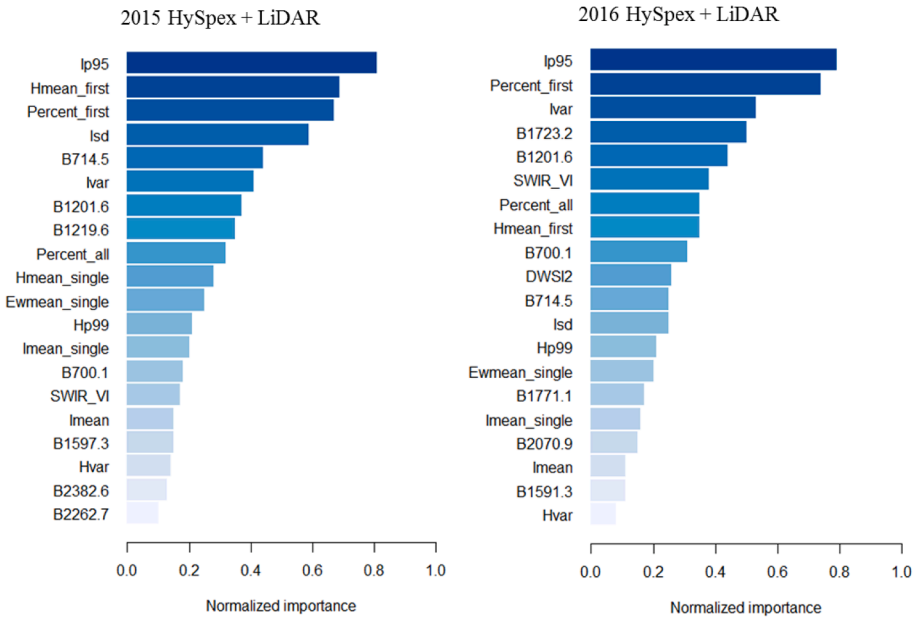

Fig. 7. The normalized importance of selected features (top 20) from the combination of each year HySpex and LiDAR data for fir classification.

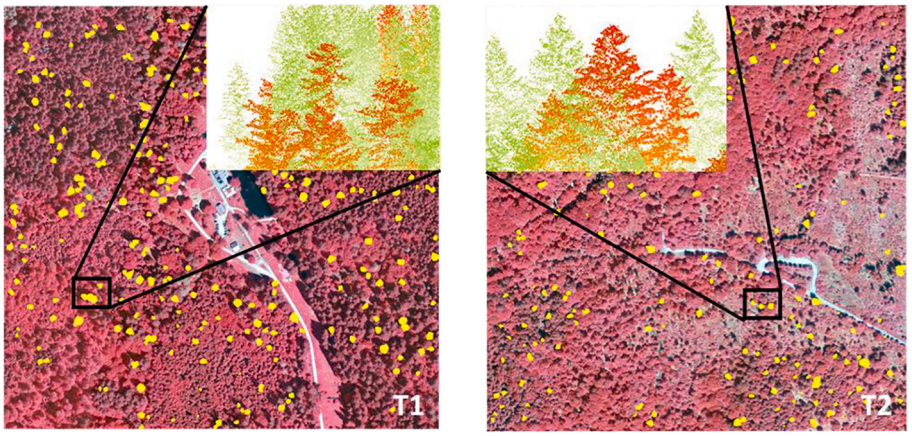

Fig. 8. Maps of fir trees in two study sites (500 m × 500 m for each site) in the Bavarian Forest National Park. The crown of fir trees are highlighted in yellow. The point clouds of mapped fir are highlighted in red. (For interpretation of the references to colour in this figure legend, the reader is referred to the web version of this article.)

Fig. 9. The crown shape of a silver fir tree (a) and a Norway spruce tree (b). (Photos by Rainer Simonis).

as the forest characteristics (e.g. homogeneity and heterogeneity).

Our results indicated that the most important LiDAR metrics for fir identification were the percentage of first returns (Percent_first) and the intensity of 95th percentile of normalized tree height (Ip95). The percentage of first returns reflects the shape of "crown shell" and the pattern of outer layers of a tree. Similarly, the intensity of 95th percentile of normalized tree height is related to the distribution of branches at the top of the canopy. From an autecological point of view, silver fir has a pyramidal crown that becomes flat-topped with age – the so-called stork's nest – while spruce displays a conic crown with an ascending upper level and drooping lower level (Farjon, 1990; Silba, 1986) (Fig. 9). The variation of the "Percent_first" captured the "flat-topped" crown traits of fir, which was the smallest among other tree species. Our results suggest that the structural differences at the top of canopy among tree species that can be captured by airborne LiDAR are valuable for tree species discrimination. Moreover, combining the complementary information from both airborne hyperspectral and LiDAR data provides additional perspectives for the discrimination of the focal species.

We did not find a significant difference between the classification results using HySpex at 4 m (2015) and HySpex at 2 m (2016) (0.03–0.06 improvement of *pu*AUC and 0.02–0.04 improvement of Kappa). The slight difference between the results may be due to the variances in illumination conditions, the number of reference pixels as well as the spatial resolution from different years. Given that the crown size of the sample trees in this study were 5–12 m, a spatial resolution smaller than the scale of tree crowns was found to be adequate for individual tree species discrimination, as also indicated by Clark et al. (2005). Our reason for using two HySpex images in this study was to evaluate the robustness of the selected features and classification methods. Given the similar acquisition date of the year and the focal species (i.e. fir as a conifer species), we did not attempt to capture phenological changes among different years for classification. However, it is notable that our study was situated in a natural temperate forest in Central Europe, the optimal spatial resolution for individual tree species mapping in other forests is closely related to the ecosystem and the focal species under consideration.

In this study, the BSVM classifier produced the highest mapping accuracies under all dataset combinations, especially in comparison to Maxent. Similar results have been reported in previous studies. For example, Waske (2017) showed that BSVM had the highest discriminative potential, followed by Maxent (with parameter tuning), Maxent (with default parameters) and OCSVM. This result is in line with Stenzel et al. (2017), who found that BSVM outperformed Maxent (with default parameters) and OCSVM in the classification of high nature value grassland areas. Although the model performance has been optimized by searching for the best combination of parameters in our study, it should be noted that input feature combinations may also influence the performance of classifiers, as mentioned by Skowronek et al. (2017). This suggests that the correlation between input features as well as the optimization of parameters within the models should be both considered for improving classification results.

Our study accurately mapped silver fir in a natural temperate forest using one-class classification, however, broadly speaking, identification and mapping of a specific tree species at the individual tree level across landscapes using remote sensing remain challenging. The mapping accuracy of the focal species is highly dependent on the tree species diversity in the study area, the similarity between the species of interest and co-existing species, and the amount of field data available. More presence and absence field data may be required before the model can be applied over a larger extent. Furthermore, as mentioned by Budei et al. (2018), having a diversity of tree ages in the sampled crowns comparatively increases the intra-species variability and the classification error probability because of the changes in tree architecture, leaf shapes and reflectance with tree age. Given the architectural variability of the top crown of fir between different ages, for example, an understanding of whether stratification by tree age or environmental factors (e.g. soil type and topographic condition) could improve classification performance should be explored in future research.

5. Conclusions

In this study, we evaluated a set of relevant spectral and structural

features derived from the hyperspectral and LiDAR data, and used them to train three one-class machine learning algorithms for individual silver fir trees mapping. Based on the results, we conclude that the biased support vector machine is the best classifier. The LiDAR intensity value of 95th percentile of normalized tree height and the percentage of first returns are the most influential structural features, capturing the main morphological difference between silver fir and Norway spruce at the top tree crown. The wavebands at 700.1 nm, 714.5 nm, and 1201.6 nm are the most important spectral bands, which are strongly affected by chlorophyll and foliar water content. Our study suggests that discovering links between spectral and structural features captured by different remotely sensed data and species-specific traits can significantly improve the mapping accuracy of a focal species at the individual tree level. The methodology we demonstrated in this study could be applied in the mapping of other tree species, which can inform management strategies to assist forest inventory in larger spatial scales and protect important species such as the silver fir.

Declaration of Competing Interest

The authors declare that they have no known competing financial interests or personal relationships that could have appeared to influence the work reported in this paper.

Acknowledgements

This work was supported by the China Scholarship Council under Grant 201506650001 and co-funded by the ITC Research Fund. We acknowledge the support of the “Data Pool Initiative for the Bohemian Forest Ecosystem” data-sharing initiative of the Bavarian Forest National Park. We would like to thank Dr. Samuel Hislop for his English editing and suggestions for this manuscript.

References

Apan, A., Held, A., Phinn, S., Markley, J., 2004. Detecting sugarcane ‘orange rust’disease using EO-1 Hyperion hyperspectral imagery. Int. J. Remote Sens. 25, 489–498.
Baldeck, C.A., Asner, G.P., 2015. Single-species detection with airborne imaging spectroscopy data: a comparison of support vector techniques. IEEE J. Sel. Top. Appl. Earth Obs. Remote Sens. 8, 2501–2512.
Baldeck, C.A., Asner, G.P., Martin, R.E., Anderson, C.B., Knapp, D.E., Kellner, J.R., Wright, S.J., 2015. Operational tree species mapping in a diverse tropical forest with airborne imaging spectroscopy. PLoS ONE 10, e0118403.
Bouvier, M., Durrieu, S., Fournier, R.A., Renaud, J.P., 2015. Generalizing predictive models of forest inventory attributes using an area-based approach with airborne LiDAR data. Remote Sens. Environ. 156, 322–334.
Budei, B.C., St-Onge, B., Hopkinson, C., Audet, F.A., 2018. Identifying the genus or species of individual trees using a three-wavelength airborne lidar system. Remote Sens. Environ. 204, 632–647.
Cailleret, M., Heurich, M., Bugmann, H., 2014. Reduction in browsing intensity may not compensate climate change effects on tree species composition in the Bavarian Forest National Park. For. Ecol. Manage. 328, 179–192.
Cho, M.A., Mathieu, R., Asner, G.P., Naidoo, L., van Aardt, J., Ramoelo, A., Debba, P., Wessels, K., Main, R., Smit, I.P.J., Erasmus, B., 2012. Mapping tree species composition in South African savannas using an integrated airborne spectral and LiDAR system. Remote Sens. Environ. 125, 214–226.
Clark, M., Roberts, D., Clark, D., 2005. Hyperspectral discrimination of tropical rain forest tree species at leaf to crown scales. Remote Sens. Environ. 96, 375–398.
Dalponte, M., Bruzzone, L., Gianelle, D., 2008. Fusion of hyperspectral and LIDAR remote sensing data for classification of complex forest areas. IEEE Trans. Geosci. Remote Sensing 46, 1416–1427.
Dalponte, M., Bruzzone, L., Gianelle, D., 2012. Tree species classification in the Southern Alps based on the fusion of very high geometrical resolution multispectral/hyperspectral images and LiDAR data. Remote Sens. Environ. 123, 258–270.
Dalponte, M., Orka, H.O., Gobakken, T., Gianelle, D., Næsset, E., 2013. Tree species classification in boreal forests with hyperspectral data. IEEE Trans. Geosci. Remote Sensing 51, 2632–2645.
Desplanque, C., Rolland, C., Schweingruber, F.H., 1999. Influence of species and abiotic factors on extreme tree ring modulation. Trees 13, 218–227.
Dobrowolska, D., Bončina, A., Klumpp, R., 2017. Ecology and silviculture of silver fir (Abies alba Mill.): a review. J. For. Res. 22, 326–335.
Elling, W., Dittmar, C., Pfaffelmoser, K., Rötzer, T., 2009. Dendroecological assessment of the complex causes of decline and recovery of the growth of silver fir (Abies alba Mill.) in Southern Germany. For. Ecol. Manage. 257, 1175–1187.
Farjon, A., 1990. Pinaceae. Drawings and descriptions of the genera Abies, Cedrus, Pseudolarix, Keteleeria, Nothotsuga, Tsuga, Cathaya, Pseudotsuga, Larix and Picea. Koeltz scientific books.
Fassnacht, F.E., Latifi, H., Stereńczak, K., Modzelewska, A., Lefsky, M., Waser, L.T., Straub, C., Ghosh, A., 2016. Review of studies on tree species classification from remotely sensed data. Remote Sens. Environ. 186, 64–87.
Ferreira, M.P., Zortea, M., Zanotta, D.C., Shimabukuro, Y.E., de Souza Filho, C.R., 2016. Mapping tree species in tropical seasonal semi-deciduous forests with hyperspectral and multispectral data. Remote Sens. Environ. 179, 66–78.
Ficko, A., Poljanec, A., Boncina, A., 2011. Do changes in spatial distribution, structure and abundance of silver fir (Abies alba Mill.) indicate its decline? For. Ecol. Manage. 261, 844–854.
Gamon, J., Surfus, J., 1999. Assessing leaf pigment content and activity with a reflectometer. The New Phytologist 143, 105–117.
Gege, P., Fries, J., Haschberger, P., Schötz, P., Schwarzer, H., Strobl, P., Suhr, B., Ulbrich, G., Jan Vreeling, W., 2009. Calibration facility for airborne imaging spectrometers. ISPRS J. Photogramm. Remote Sens. 64, 387–397.
Gitelson, A.A., Gritz, Y., Merzlyak, M.N., 2003. Relationships between leaf chlorophyll content and spectral reflectance and algorithms for non-destructive chlorophyll assessment in higher plant leaves. J. Plant Physiol. 160, 271–282.
Heinzel, J., Koch, B., 2011. Exploring full-waveform LiDAR parameters for tree species classification. Int. J. Appl. Earth Obs. Geoinf. 13, 152–160.
Heinzel, J., Koch, B., 2012. Investigating multiple data sources for tree species classification in temperate forest and use for single tree delineation. Int. J. Appl. Earth Obs. Geoinf. 18, 101–110.
Heurich, M., Beudert, B., Rall, H., Křenová, Z., 2010. National parks as model regions for interdisciplinary long-term ecological research: the Bavarian Forest and Šumavá National Parks underway to transboundary ecosystem research. Long-Term Ecological Research, Springer, pp. 327–344.
Heurich, M., Englmaier, K.H., 2010. The development of tree species composition in the Rachel-Lusen region of the Bavarian Forest National Park. Silva Gabreta 16, 165–186.
Huber, S., Kneubuhler, M., Psomas, A., Itten, K., Zimmermann, N.E., 2008. Estimating foliar biochemistry from hyperspectral data in mixed forest canopy. For. Ecol. Manage. 256, 491–501.
Klopčič, M., Mina, M., Bugmann, H., Bončina, A., 2017. The prospects of silver fir (Abies alba Mill.) and Norway spruce (Picea abies (L.) Karst) in mixed mountain forests under various management strategies, climate change and high browsing pressure. Eur. J. Forest Res. 136, 1071–1090.
Kokaly, R.F., Asner, G.P., Ollinger, S.V., Martin, M.E., Wessman, C.A., 2009. Characterizing canopy biochemistry from imaging spectroscopy and its application to ecosystem studies. Remote Sensing Environ. 113 (Suppl. 1), S78–S91.
Korpela, I., Ørka, H.O., Maltamo, M., Tokola, T., Hyyppä, J., 2010. Tree species classification using airborne LiDAR–effects of stand and tree parameters, downsizing of training set, intensity normalization, and sensor type. Silva Fennica 44, 319–339.
Li, J., Hu, B., Noland, T.L., 2013. Classification of tree species based on structural features derived from high density LiDAR data. Agric. For. Meteorol. 171–172, 104–114.
Lin, Y., Herold, M., 2016. Tree species classification based on explicit tree structure feature parameters derived from static terrestrial laser scanning data. Agric. For. Meteorol. 216, 105–114.
Lin, Y., Hyyppä, J., 2016. A comprehensive but efficient framework of proposing and validating feature parameters from airborne LiDAR data for tree species classification. Int. J. Appl. Earth Obs. Geoinf. 46, 45–55.
Liu, B., Dai, Y., Li, X., Lee, W.S., Yu, P.S., 2003. Building text classifiers using positive and unlabeled examples. In: Third IEEE International Conference on Data Mining, pp. 179–186.
Liu, J., Skidmore, A.K., Jones, S., Wang, T., Heurich, M., Zhu, X., Shi, Y., 2018. Large off-nadir scan angle of airborne LiDAR can severely affect the estimates of forest structure metrics. ISPRS J. Photogramm. Remote Sens. 136, 13–25.
Lobell, D.B., Asner, G.P., Law, B.E., Treuhaft, R.N., 2001. Subpixel canopy cover estimation of coniferous forests in Oregon using SWIR imaging spectrometry. J. Geophys. Res.: Atmos. 106, 5151–5160.
Mack, B., 2015. oneClass: One-Class Classification in the Absence of Test Data, Version 0.1-1: Software. In.
Mack, B., Roscher, R., Waske, B., 2014. Can i trust my one-class classification? Remote Sensing 6, 8779–8802.
Mack, B., Waske, B., 2017. In-depth comparisons of MaxEnt, biased SVM and one-class SVM for one-class classification of remote sensing data. Remote Sensing Lett. 8, 290–299.
Maldonado, S., Weber, R., 2009. A wrapper method for feature selection using Support Vector Machines. Inf. Sci. 179, 2208–2217.
Marrs, J., Ni-Meister, W., 2019. Machine learning techniques for tree species classification using co-registered LiDAR and hyperspectral data. Remote Sensing 11, 819.
Merton, R., 1998. Monitoring community hysteresis using spectral shift analysis and the red-edge vegetation stress index. In: Proceedings of the Seventh Annual JPL Airborne Earth Science Workshop, pp. 12–16.
Müller, R., Lehner, M., Reinartz, P., Schroeder, M., 2005. Evaluation of spaceborne and airborne line scanner images using a generic ortho image processor. In: Proc. of High Resolution Earth Imaging for Geospatial Information, ISPRS Hannover Workshop, Commision I WG (p. 2005).
Muñoz-Marí, J., Bovolo, F., Gómez-Chova, L., Bruzzone, L., Camp-Valls, G., 2010. Semisupervised one-class support vector machines for classification of remote sensing data. IEEE Trans. Geosci. Remote Sens. 48, 3188–3197.

Muss, J.D., Mladenoff, D.J., Townsend, P.A., 2011. A pseudo-waveform technique to assess forest structure using discrete lidar data. Remote Sens. Environ. 115, 824–835.
Ørka, H.O., Dalponte, M., Gobakken, T., Næsset, E., Ene, L.T., 2013. Characterizing forest species composition using multiple remote sensing data sources and inventory approaches. Scand. J. For. Res. 28, 677–688.
Pearson, R.G., 2007. Species' distribution modeling for conservation educators and practitioners. Synthesis. Am. Museum Nat. History 50, 54–89.
Phillips, S.J., Anderson, R.P., Schapire, R.E., 2006. Maximum entropy modeling of species geographic distributions. Ecol. Model. 190, 231–259.
Phillips, S.J., Dudík, M., 2008. Modeling of species distributions with Maxent: new extensions and a comprehensive evaluation. Ecography 31, 161–175.
Piiroinen, R., Fassnacht, F.E., Heiskanen, J., Maeda, E., Mack, B., Pellikka, P., 2018. Invasive tree species detection in the Eastern Arc Mountains biodiversity hotspot using one class classification. Remote Sens. Environ. 218, 119–131.
Puttonen, E., Suomalainen, J., Hakala, T., Räikkönen, E., Kaartinen, H., Kaasalainen, S., Litkey, P., 2010. Tree species classification from fused active hyperspectral reflectance and LIDAR measurements. For. Ecol. Manage. 260, 1843–1852.
Richter, R., Reu, B., Wirth, C., Doktor, D., Vohland, M., 2016. The use of airborne hyperspectral data for tree species classification in a species-rich Central European forest area. Int. J. Appl. Earth Obs. Geoinf. 52, 464–474.
Richter, R., Schläpfer, D., 2002. Geo-atmospheric processing of airborne imaging spectrometry data. Part 2: atmospheric/topographic correction. Int. J. Remote Sens. 23, 2631–2649.
Schläpfer, D., Richter, R., 2011. Spectral polishing of high resolution imaging spectroscopy data. In: Proceedings of the 7th SIG-IS Workshop on Imaging Spectroscopy, Edinburgh, UK, pp. 11–13.
Schölkopf, B., Burges, C.J., Smola, A.J., 1999. Advances in Kernel Methods: Support Vector Learning. MIT press.
Schwind, P., Schneider, M., Müller, R., 2014. Improving HySpex sensor Co-registration accuracy using BRISK and sensor-model based RANSAC. Int. Arch. Photogrammetry, Remote Sensing Spatial Inform. Sci. 40, 371.
Senn, J., Suter, W., 2003. Ungulate browsing on silver fir (Abies alba) in the Swiss Alps: beliefs in search of supporting data. For. Ecol. Manage. 181, 151–164.
Sethna, J., 2006. Statistical Mechanics: Entropy, Order Parameters, and Complexity. Oxford University Press.
Shi, Y., Skidmore, A.K., Wang, T., Holzwarth, S., Heiden, U., Pinnel, N., Zhu, X., Heurich, M., 2018a. Tree species classification using plant functional traits from LiDAR and hyperspectral data. Int. J. Appl. Earth Obs. Geoinf. 73, 207–219.
Shi, Y., Wang, T., Skidmore, A.K., Heurich, M., 2018b. Important LiDAR metrics for discriminating forest tree species in Central Europe. ISPRS J. Photogramm. Remote Sens. 137, 163–174.
Silba, J., 1986. Encyclopaedia coniferae. Phytologia memoirs. Vol. VIII. Moldenke and Moldenke, Corvallis, Oreg.
Simard, M., Saatchi, S.S., De Grandi, G., 2000. The use of decision tree and multiscale texture for classification of JERS-1 SAR data over tropical forest. IEEE Trans. Geosci. Remote Sens. 38, 2310–2321.
Skowronek, S., Asner, G.P., Feilhauer, H., 2017. Performance of one-class classifiers for invasive species mapping using airborne imaging spectroscopy. Ecol. Inf. 37, 66–76.
Skowronek, S., Van De Kerchove, R., Rombouts, B., Aerts, R., Ewald, M., Warrie, J., Schiefer, F., Garzon-Lopez, C., Hattab, T., Honnay, O., Lenoir, J., Rocchini, D., Schmidtlein, S., Somers, B., Feilhauer, H., 2018. Transferability of species distribution models for the detection of an invasive alien bryophyte using imaging spectroscopy data. Int. J. Appl. Earth Obs. Geoinf. 68, 61–72.
Somers, B., Asner, G.P., 2013a. Invasive species mapping in Hawaiian rainforests using multi-temporal hyperion spaceborne imaging spectroscopy. IEEE J. Sel. Top. Appl. Earth Obs. Remote Sens. 6, 351–359.
Somers, B., Asner, G.P., 2013b. Multi-temporal hyperspectral mixture analysis and feature selection for invasive species mapping in rainforests. Remote Sens. Environ. 136, 14–27.
Somers, B., Asner, G.P., 2014. Tree species mapping in tropical forests using multi-temporal imaging spectroscopy: wavelength adaptive spectral mixture analysis. Int. J. Appl. Earth Obs. Geoinf. 31, 57–66.
Stenzel, S., Fassnacht, F.E., Mack, B., Schmidtlein, S., 2017. Identification of high nature value grassland with remote sensing and minimal field data. Ecol. Ind. 74, 28–38.
Suratman, M.N., 2012. Tree species diversity and forest stand structure of Pahang National Park. INTECH Open Access Publisher, Malaysia.
Tinner, W., Colombaroli, D., Heiri, O., Henne, P.D., Steinacher, M., Untenecker, J., Vescovi, E., Allen, J.R., Carraro, G., Conedera, M., 2013. The past ecology of Abies alba provides new perspectives on future responses of silver fir forests to global warming. Ecol. Monogr. 83, 419–439.
Ustin, S.L., Gitelson, A.A., Jacquemoud, S., Schaepman, M., Asner, G.P., Gamon, J.A., Zarco-Tejada, P., 2009. Retrieval of foliar information about plant pigment systems from high resolution spectroscopy. Remote Sensing of Environment 113 (Suppl. 1), S67–S77.
Vaglio Laurin, G., Cheung-Wai Chan, J., Chen, Q., Lindsell, J.A., Coomes, D.A., Guerriero, L., Del Frate, F., Miglietta, F., Valentini, R., 2014. Biodiversity mapping in a tropical West African forest with airborne hyperspectral data. PLoS ONE 9, e97910.
Vallet, P., Pérot, T., 2011. Silver fir stand productivity is enhanced when mixed with Norway spruce: evidence based on large-scale inventory data and a generic modelling approach. J. Veg. Sci. 22, 932–942.
Vauhkonen, J., Korpela, I., Maltamo, M., Tokola, T., 2010. Imputation of single-tree attributes using airborne laser scanning-based height, intensity, and alpha shape metrics. Remote Sens. Environ. 114, 1263–1276.
Vauhkonen, J., Ørka, H.O., Holmgren, J., Dalponte, M., Heinzel, J., Koch, B., 2014. Tree species recognition based on airborne laser scanning and complementary data sources. Forestry Applications of Airborne Laser Scanning, Springer, pp. 135–156.
Vrška, T., Adam, D., Hort, L., Kolář, T., Janík, D., 2009. European beech (Fagus sylvatica L.) and silver fir (Abies alba Mill.) rotation in the Carpathians—a developmental cycle or a linear trend induced by man? For. Ecol. Manage. 258, 347–356.
Wagner, W., Ullrich, A., Ducic, V., Melzer, T., Studnicka, N., 2006. Gaussian decomposition and calibration of a novel small-footprint full-waveform digitising airborne laser scanner. ISPRS J. Photogramm. Remote Sens. 60, 100–112.
Waske, B., 2017. In-depth comparisons of MaxEnt, biased SVM and one-class SVM for one-class classification of remote sensing data AU - Mack, Benjamin. Remote Sensing Lett. 8, 290–299.
Yao, W., Krzystek, P., Heurich, M., 2012. Tree species classification and estimation of stem volume and DBH based on single tree extraction by exploiting airborne full-waveform LiDAR data. Remote Sens. Environ. 123, 368–380.
Yao, W., Krzystek, P., Heurich, M., 2013. Enhanced detection of 3D individual trees in forested areas using airborne full-waveform LiDAR data by combining normalized cuts with spatial density clustering. ISPRS Annals of Photogram., Remote Sensing Spatial Inform. Sci. 1, 349–354.
Yin, D., Wang, L., 2016. How to assess the accuracy of the individual tree-based forest inventory derived from remotely sensed data: a review. Int. J. Remote Sens. 37, 4521–4553.